Chemical Science

EDGE ARTICLE

View Article Online
View Journal | View Issue



Cite this: *Chem. Sci.*, 2015, **6**, 425

# Stepwise isolation of low-valent, low-coordinate Sn and Pb mono- and dications in the coordination sphere of platinum†

Holger Braunschweig,*[a] Mehmet Ali Celik,[a] Rian D. Dewhurst,[a] Magdalena Heid,[a] Florian Hupp[a] and Sakya S. Sen[b]

Received 24th September 2014
Accepted 15th October 2014

DOI: 10.1039/c4sc02948h

www.rsc.org/chemicalscience

Synthetic access to low-coordinate Pb mono- and dications is in general impeded due to their poor solubility and highly electrophilic nature. However, the electrophilicity of these cations can be tamed by attaching them to electron-rich transition metals. Following this principle we have isolated low-valent Pb mono- ($[(Cy_3P)_2Pt{-}PbCl]_2[AlCl_4]_2$, **8a**) and dications ($[(Cy_3P)_2Pt(Pb)][AlCl_4]_2$, **11**) in the coordination sphere of platinum. The same approach then has been implemented for the isolation of analogous low-valent Sn mono- (**7a**) and dications (**10**). An energy decomposition analysis (EDA-NOCV) was performed to investigate the nature of Pt–Pb and Pb–Cl bonding in $[(Cy_3P)_2Pt(PbCl_2)]$ (**2**), **8a** and **11**. The results show that the Pt–Pb bonds in **8a** and **11** are electron-sharing in nature, whereas that of the precursor **2** is a dative bond. The breakdown of attractive interactions in **2**, **8a** and **11** reveals that the ionic interactions in the analyzed Pt–Pb and Pb–Cl bonds are always stronger than the covalent interactions, except for the Pb–Cl bond in **8a**. The calculated D3 dispersion energies show that dispersion interactions play a key role in the thermodynamic stability of **2**, **8a** and **11**.

## Introduction

Following the isolation of a series of cations of composition $[(C_5Me_5)E{:}]^+$ (E = Si–Pb) by Jutzi and co-workers,[1] the synthesis and structural elucidation of divalent group 14 cations and dications has become a subject of considerable current interest. Recent isolation of a Ge(II) dication encapsulated within a cryptand (**A**, Scheme 1) by Baines *et al.* and carbodiphosphorane-stabilized $[GeCl]^+$ (**B**) and $[(SnCl)_2]^{2+}$ (**C**) accentuates the ongoing growth of the chemistry of tetrylene(ii) cations.[2,3] Much of this interest stems from the fact that the central atom in these salts carries two unoccupied valence orbitals as well as a lone pair of electrons. Such an electronic description suggests ambiphilicity, making them potentially interesting candidates for noninnocent (*i.e.* both σ-donating and π-accepting) ligation to transition metals – a topic of great interest for catalysis. Accordingly, the successful synthesis of divalent group 14 cations has required the design of new synthetic strategies based upon sterically-demanding neutral (cryptand, N-heterocyclic carbene, carbodiphosphorane) or monoanionic (β-diketiminate, cyclopentadienyl, *N*-isopropyl-2-(isopropylamino)troponimine, cyclophane, *etc.*) ligands, the utilization of counteranions, and solvents with low nucleophilicity in order to avoid their coordination to the cation. Noteworthy in this context is the work of the groups of Baines, Driess, Jones, Müller, Krossing, and others who have reported a plethora of such species.[4–13]

In stark contrast to the foregoing, only a handful of low-coordinate lead(II) cations have been experimentally realized. Their isolation at ambient temperature is hindered by the highly electrophilic nature of these species. Jutzi and Nöth reported the first cationic Pb(II) compounds of the type $[\eta^5\text{-Cp*Pb}]^+X^-$ (**D**) (X = $BF_4$ and $OSO_2CF_3$).[14] Following this, Power published the synthesis of a lead(II) cation supported by a bulky terphenyl substituent (**E**), which is weakly coordinated by a toluene molecule.[15] Very recently, Fulton and co-workers isolated two more Pb(II) cations stabilized by bulky β-diketiminato ligands.[16] Apart from these, a few dications of lead have been realized through σ- or π-donating (N–, O–, or S–) atoms or by chelating ligands such as tmeda, bipyridine *etc.*[17–19] Higher-coordinate lead(II) dications with weak arene interactions stabilized by chloride anions are also known,[20,21] for example $[(1,2\text{-}C_6H_4Me_2)_2Pb(AlCl_4)_2]$ (**F**).[22] However, such stabilization occurs at the expense of the degree of the cationic character of the Pb atom, thus leading to an increase in its coordination number (six to eight). As a result, such species cannot be classified as low-coordinate cations. In order to realize a $[LPb\text{-}Cl]^+$ or $[LPb]^{2+}$ moiety, the use of a neutral ligand such as

[a]*Institut für Anorganische Chemie, Julius-Maximilians-Universität Würzburg, Am Hubland, 97074 Würzburg, Germany; Web: http://www-anorganik.chemie.uni-wuerzburg.de/Braunschweig/. E-mail: h.braunschweig@uni-wuerzburg.de*

[b]*CSIR-National Chemical Laboratory, Pashan, Pune 411008, India*

† Electronic supplementary information (ESI) available: Experimental and synthetic procedures, characterisation data, computational details, and crystallographic methods employed in this work are given. CCDC 1002025–1002028 and 1023363–1023368. For ESI and crystallographic data in CIF or other electronic format see DOI: 10.1039/c4sc02948h

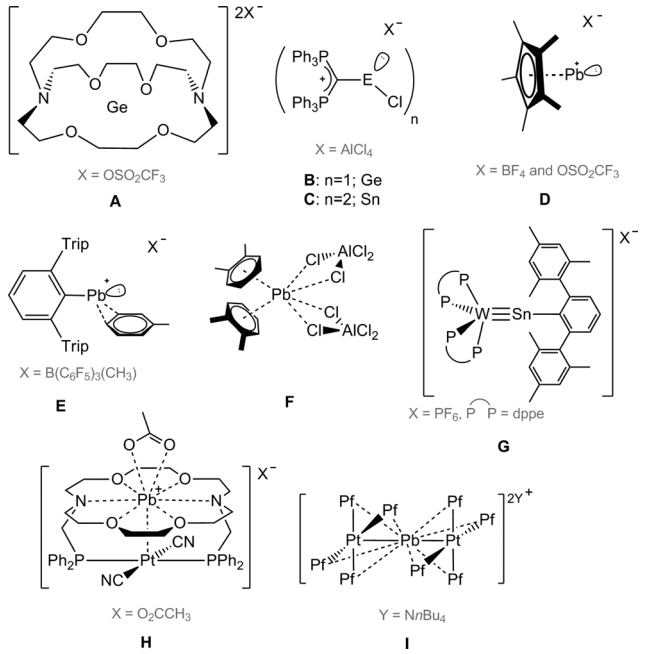


Scheme 1 Selected cationic complexes of heavier group 14 elements.

N-heterocyclic carbenes, carbodiphosphoranes or others seems logical, as they do not contribute to the formal charge or oxidation state of the central atom. However, to the best of our knowledge, reports of cationic lead(II) compounds containing such ligands have thus far not appeared (Scheme 1).

It was only recently that Filippou *et al.* reported another approach, in which the coordination sphere of late transition metals was employed to stabilize germanium(II)[23] and tin(II) cations. Thereby, complexes such as $[(Ph_2PCH_2CH_2PPh_2)_2WSn–C_6H_3\text{-}2,6\text{-}Mes_2][PF_6]$ (**G**),[24] as well as the molybdenum plumbylidyne complex *trans*-$[Br(Me_3P)_4MoPb(C_6H_3\text{-}2,6\text{-}Trip_2)]$ (Trip = 2,4,6-$iPr_3$-$C_6H_2$),[25] among others, were isolated. A few lead(II) dications in the coordination sphere of a late transition metal have been reported, albeit stabilized by chelating N-, and O-donor ligands (phenanthroline and diaza-18-crown-6)[26] such as $[(CH_3CO_2)Pb(crown\text{-}P_2)Pt(CN)_2][(O_2CCH_3)]$ (**H**),[27] or $[\{Pt(C_6F_5)_4\}_2(Pb)][nBu_4N]_2$ (**I**) showing interaction with numerous fluorine atoms.[28]

Our aim was to establish a transition metal scaffold that would stabilize low-coordinate Sn(II) and Pb(II) cations and dications. Consequently, we turned our attention towards the electron-rich, coordinatively unsaturated complex $[(Cy_3P)_2Pt]$ (**1**) as it (i) has shown an impressive ability to stabilize reactive main-group species, such as diborenes,[29] cationic boryl and borylene complexes,[30–33] and iminoboryl, oxoboryl, and alkylideneboryl complexes;[34–38] and (ii) is now well-established as a strong and synthetically-convenient transition metal Lewis base.[39–46]

## Results and discussion

As part of our recent work to delineate the concept of metal-only Lewis Pairs (MOLPs),[39–46] we recently reported the mono- and diplatinum plumbylene complexes $[(Cy_3P)_2Pt–PbCl_2]_2$ (**2**) and $[\{(Cy_3P)_2Pt\}_2PbCl_2]$ (**3**).[47] By qualitative inspection of the calculated frontier orbitals of these complexes, we had surmised the existence of σ donation both from Pt to Pb and from Pb to Pt, a phenomenon we described as synergic σ-donation.[47] Subsequent DFT calculations indicated that similar bonding patterns exist in transition metal complexes containing multiple bonds between Group 10/14 elements.[48] The qualitative EDA calculations done in this work, however, call this description into question (*vide infra*).

In order to synthesize the analogous stannylene complex, we reacted stoichiometric amounts of tin(II) bromide with **1**, which resulted in the formation of $[(Cy_3P)_2Pt–SnBr_2]$ (**4**) in near-quantitative yields. Likewise, the diplatinum species $[\{(Cy_3P)_2Pt\}_2SnBr_2]$ (**5**) can be readily synthesized by addition of two equivalents of **1** to $SnBr_2$ (Scheme 2).

The progress of the reactions was indicated by their color change from colorless (**1**) to violet-red (**4**) and purple-red (**5**), respectively. The $^{31}P\{^1H\}$ NMR spectra of the complexes revealed sharp singlets at $\delta = 49.7$ ppm ($^1J_{P–Pt} = 3421$ Hz) for **4** and at $\delta = 50.7$ ppm ($^1J_{P–Pt} = 4197$ Hz) for **5**, which are slightly upfield-shifted in comparison to that of **1** ($\delta = 62.3$ ppm, $^1J_{P–Pt} = 4164$ Hz). All attempts to detect $^{119}Sn\{^1H\}$ NMR resonances failed, presumably due to an increased electric field gradient and large chemical shift anisotropy at the $^{119}Sn$ site.[49,50] The $^{195}Pt\{^1H\}$ NMR spectrum of **4** and **5** reveal triplets at $\delta = -4903$ ppm ($^1J_{P–Pt} = 3421$ Hz) and at $\delta = -5239$ ppm ($^1J_{P–Pt} = 4197$ Hz), respectively. The frequencies of the resonances and the change in the coupling constants is in accordance with those of previously reported plumbylene analogues.[47]

Both complexes **4** and **5** exhibit T-shaped geometry around the platinum center (Fig. 1). In contrast to the heavier lead analogue **2**, compound **4** is not dimeric. The metal–metal distances $d_{MM}$ are compared with the sum of the experimentally derived radii of the atoms involved, $\sum_{covrad}$, as sourced from a survey of the Cambridge Crystallographic Database. The resulting ratio, a useful tool for comparison of different dative bond lengths, is denoted $d_{rel}$.[46] The Pt–Sn distances of the monoplatinum complex **4** (Pt1–Sn1 2.605(1) Å, $d_{rel} = 0.947$) and the diplatinum complex **5** (Pt1–Sn1 2.643(1) Å, $d_{rel} = 0.961$; Pt2–Sn1 2.657(1) Å, $d_{rel} = 0.966$) are very similar, and very similar $d_{rel}$ values have been observed in the heavier lead analogues (**2**: $d_{rel} = 0.968$, **3**: $d_{rel} = 0.981$, 0.989) and other

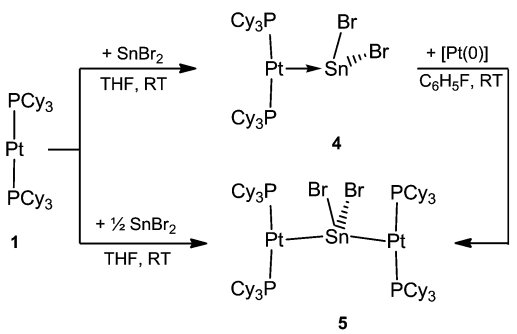


Scheme 2 Formation of the stannylene complexes **4** and **5**.

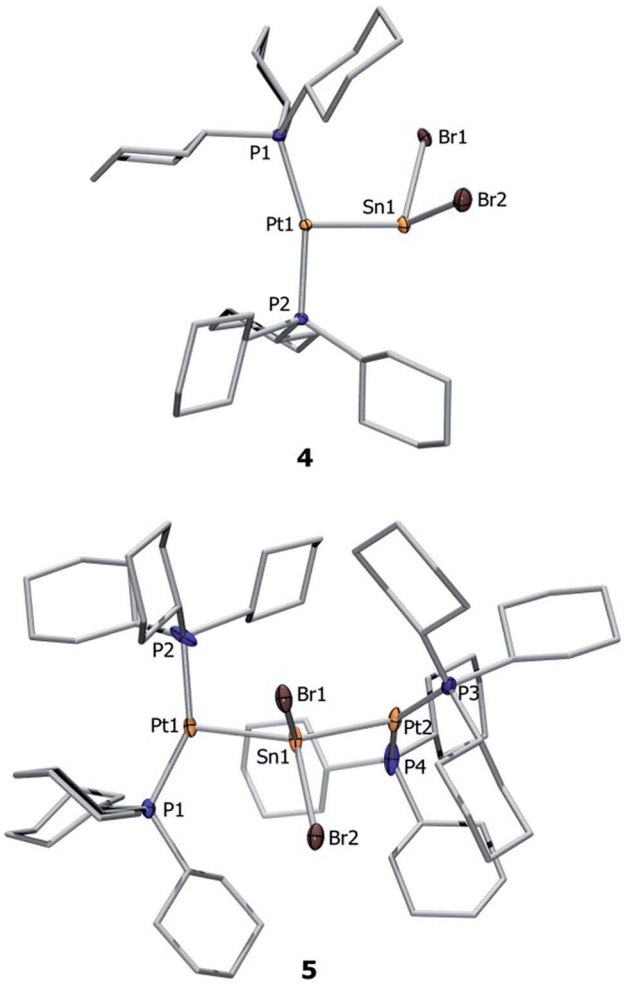


Fig. 1 Molecular structures of **4** and **5**. Ellipsoids are drawn at the 50% probability level. Hydrogen atoms, solvent molecules and ellipsoids of the cyclohexyl rings are omitted for clarity. Selected bond lengths [Å] and angles [°]: **4**: Pt–Sn 2.605(2), Sn–Br1 2.654(1), Sn–Br2 2.626(2), P1–Pt–P2 160.1(1), Br1–Sn–Br2 96.1(1), Pt–Sn–Br1 112.0(1), Pt–Sn–Br2 102.3(1). **5**: Pt1–Sn1 2.643(1), Pt2–Sn1 2.657(1), Sn1–Br1 2.674(1), Sn1–Br2 2.661(1), Pt1–Sn1–Pt2 139.0(1), Br1–Sn1–Br2 88.1(1), P2–Pt1–Sn3 100.4(1), P1–Pt1–Sn1–Br2 12.0(1), P1–Pt1–Sn1–Br1 102.3(1).

known tin(II) halide-bridged transition metal complexes *e.g.* $[\{(Me_3P)_3ClRh\}_2(\mu\text{-}SnCl_2)]$ (**6**) ($d_{rel}$ = 0.965, 0.968).[47,51] The Pt–Sn–Pt angle of **5** (139.0(1)°) matches well with the diplatinum Pb complex **3** (140.1(1)°) and Marder's dirhodium species (142.5(1)°).[51] Characteristic NMR and structural data for the neutral and cationic stannylene and plumbylene complexes are summarized in Table 1.

### Synthesis of low-valent Sn and Pb monocations

It was envisaged that divalent group 14 MOLPs may act as ideal precursors for the synthesis of low-coordinate group 14 cations, *via* halide abstraction. Stoichiometric addition of $AlBr_3$ or Na $[BAr^{Cl}{}_4]$ [$Ar^{Cl}$ = 3,5-$Cl_2$-$C_6H_3$] to monoplatinum stannylene complex **4** and plumbylene complex **2** resulted in new cationic complexes $[(Cy_3P)_2Pt(SnBr)]_2[X]_2$ (**7a** = $AlBr_4$, **7b** = $BAr^{Cl}{}_4$), and $[(Cy_3P)_2Pt\text{–}PbCl]_2[X]_2$ (**8a** = $AlBr_4$, **8b** = $BAr^{Cl}{}_4$) (Scheme 3). In order to prevent halogen exchange between the MOLPs and aluminium halides, $AlBr_3$ was chosen as halide abstracting agent for bromostannylene **4**, and $AlCl_3$ for the chloroplumbylene **2**.

All of these cations were characterized by multinuclear NMR spectroscopy and X-ray structural analysis. For all complexes, the $^{31}P\{^1H\}$ NMR spectrum shows a sharp singlet flanked by $^{195}Pt$ satellites (**7a**: $\delta$ = 49.3 ppm, $^1J_{P\text{–}Pt}$ = 3097 Hz; **7b**: $\delta$ = 49.4 ppm, $^1J_{P\text{–}Pt}$ = 3104 Hz; **8a**: $\delta$ = 46.6 ppm, $^1J_{P\text{–}Pt}$ = 3100 Hz; **8b**: $\delta$ = 46.7 ppm, $^1J_{P\text{–}Pt}$ = 3115 Hz). In comparison to the precursor there is almost no change of the chemical shift value (**4**: $\delta$ = 49.6 ppm, $^1J_{P\text{–}Pt}$ = 3421 Hz; **2**: $\delta$ = 48.3 ppm, $^1J_{P\text{–}Pt}$ = 3450 Hz). However, the decrease of the $^{31}P\text{–}^{195}Pt$ coupling constants is a strong indicator of the formation of cationic complexes, as similar decreases were observed during the formation of platinum-boryl cations of the form *trans*-$[(Cy_3P)_2Pt(MeCN)\{BBr(NMe_2)\}][BAr^F{}_4]$ (**9**).[52] The $^{27}Al$ NMR spectrum reveals a broad singlet at $\delta$ = 80.8 ppm which is quite common for a tetrahedral aluminate.[53] All attempts to detect $^{119}Sn\{^1H\}$, $^{207}Pb\{^1H\}$, or $^{195}Pt\{^1H\}$ NMR resonances of **7a,b** and **8a,b** (and, in fact, all of the complexes prepared herein) failed despite the use of wide spectral widths. This is presumably due to increased electric field gradient and large chemical shift anisotropy at the heavy tetrel element site, in addition to the extensive coupling with other NMR-active nuclei.[49,50,54,55] This is in line with the well-documented difficulties in detecting $^{11}B$ NMR signals in related cationic borylene complexes of the form $[(Cy_3P)_2Pt(BRL_n)]^+$ ($n$ = 0, 1).[30,32,33,52]

Orange crystals of **7a/b** were grown by diffusion of hexanes into a $CH_2Cl_2$ solution at −40 °C and were analyzed by single-crystal X-ray diffraction. As the dication of **7a** is centrosymmetric and the dications of **7a/b** are identical, only the structural features of **7b** are discussed here. Complex **7b** features a slightly distorted T-shaped geometry around the platinum atom (Fig. 2). In the solid-state structure, the borate anion and tin cation are clearly separated, the shortest Sn···Cl(WCA) distance being 4.020(1) Å (WCA = weakly coordinating anion). This is not only longer than the longest Sn···Cl(WCA) distance in **C** (3.527 Å), but also than the sum of their van der Waals radii (3.92 Å).[56] The Pt–Sn distances in **7b** (2.524(2) Å) are significantly shorter than that of the starting material (**4**: 2.605(2) Å).

The X-ray-derived structural features of **8a** are discussed here and the structural features of **8b** are provided in the ESI.† Complex **8a** crystallizes in the orthorhombic space group $Pca2_1$ (Fig. 2). In the solid-state structure of **8a**, the tetrachloroaluminate anion and lead atoms are loosely associated, the shortest Pb···Cl(WCA) distance being 3.420(1) Å, which is much shorter than the sum of their van der Waals radii (3.77 Å).[56] This long contact is in contrast to **7a**, the cation of which shows complete separation from its WCA ($[BAr^{Cl}{}_4]^-$). The complex features a slightly distorted T-shaped geometry around the platinum atom. As in the previous case, the Pt–Pb bonds (2.603(1) Å) are shorter than those of the precursor (**2**: 2.730(1) Å).

### Synthesis of low-valent Sn and Pb dications

Naked divalent dications of tetrel elements are presumably far too unstable to be isolated. However, we reasoned that

Table 1 NMR data and bond lengths of neutral, mono-, and dicationic Sn and Pb complexes prepared herein

| Substance | $^{31}P\{^1H\}^a$ | $^1J_{P-Pt}{}^b$ | Pt–M[c] | M–X[c] |
|---|---|---|---|---|
| $[(Cy_3P)_2Pt(PbCl_2)]$ (**2**)[47] | 48.3 | 3450 | 2.730(1) | 2.619(1), 3.139(1) |
| $[\{(Cy_3P)_2Pt\}_2PbCl_2]$ (**3**)[47] | 50.4 | 4032 | 2.767(1), 2.789(1) | 2.628(1), 2.616(1) |
| $[(Cy_3P)_2Pt(SnBr_2)]$ (**4**) | 49.7 | 3421 | 2.605(2) | 2.654(1), 2.626(2) |
| $[\{(Cy_3P)_2Pt\}_2SnBr_2]$ (**5**) | 50.7 | 4197 | 2.643(1), 2.657(1) | 2.674(1), 2.661(1) |
| $[(Cy_3P)_2Pt(SnBr)][AlBr_4]$ (**7a**) | 49.9 | 3130 | | |
| $[(Cy_3P)_2Pt(SnBr)][BAr^{Cl}{}_4]$ (**7b**) | 49.4 | 3104 | 2.524(1) | 2.780(1), 2.821(1) |
| $[(Cy_3P)_2Pt(PbCl)][AlCl_4]$ (**8a**) | 46.6 | 3099 | 2.603(1) | 2.769(3), 2.822(3) |
| $[(Cy_3P)_2Pt(PbCl)][BAr^{Cl}{}_4]$ (**8b**) | 46.7 | 3115 | | |
| $[(Cy_3P)_2Pt(Sn)][AlBr_4]_2$ (**10**) | 52.1 | 3021 | 2.502(1) | 3.155(1), 3.264(1), 2.956(1) |
| $[(Cy_3P)_2Pt(Pb)][AlCl_4]_2$ (**11**) | 47.5 | 2950 | 2.564(1) | |
| $[N(nBu)_4][(Cy_3P)_2Pt(SnBr_3)]$ (**16**) | 56.5 | 4634 | 2.604(1) | |
| $[(Cy_3P)_2Pt(PbCl)(4\text{-}Me\text{-}C_5H_4N)][AlCl_4]$ (**17**) | 47.1 | 3350 | | |
| $[(Cy_3P)_2Pt(PbI)][AlCl_4]$ (**18**) | 45.5 | 3130 | 2.619(1) | 2.917(2), 3.092(2) |
| $[(Cy_3P)_2Pt(PbClBr)]$ (**19**) | 48.2 | 3520 | | |

[a] $\delta$ in ppm. [b] Coupling constants in Hz. [c] Distances in Å.

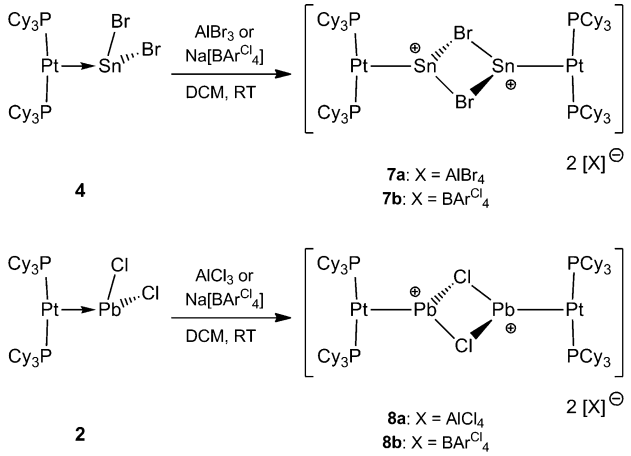


Scheme 3 Formation of dicationic diplatinum complexes of $Sn_2Br_2$ (**7a** and **7b**) and $Pb_2Br_2$ (**8a** and **8b**).

abstraction of two chlorides from **2** or **4** may provide simple, monocoordinate, low-valent Sn or Pb dications if the strongly Lewis basic nature of the metal center can be harnessed to partly relieve the electron deficiency of such a dication. The greater extent of Pt–M (M = Sn, Pb) σ donation in **7a** and **8a** over that in **4** and **2** might provide enough electronic stabilization to attenuate the reactivity of the M dication and allow its isolation. Addition of two equivalents of $AlBr_3$ to **4** and $AlCl_3$ to **2** resulted in the formation of the loosely-associated salts $[(Cy_3P)_2Pt(Sn)][AlBr_4]_2$ (**10**) and $[(Cy_3P)_2Pt(Pb)][AlCl_4]_2$ (**11**) (Scheme 4). Alternatively, halide abstraction from **7a** and **8a** using stoichiometric amounts of $AlBr_3$ or $AlCl_3$ also led to the desired dicationic species **10** and **11**, respectively.

The $^{31}P\{^1H\}$ NMR spectrum of compound **10** reveals a sharp singlet with $^{195}Pt$ satellites at $\delta = 52.9$ ppm ($^1J_{P-Pt} = 2993$ Hz), marginally downfield from that of **4** ($\delta = 49.7$ ppm, $^1J_{P-Pt} = 3421$ Hz). In contrast to **10**, the low-valent Pb dicationic complex **11** exhibits a resonance ($\delta = 47.5$ ppm, $^1J_{P-Pt} = 2950$ Hz) marginally upfield of that of **2**. However, the decrease of the coupling constants from the neutral species as well as from **7a**/**8a** indicates the formation of a dicationic species. The $^{27}Al$ NMR spectra of **10** and **11** reveal broad singlets at $\delta = 80.8$ and 103.6 ppm, respectively, indicating a tetrahedral aluminate.[53] No $^{119}Sn\{^1H\}$ or $^{207}Pb\{^1H\}$ NMR resonances were detected despite several attempts.

Single crystal X-ray diffraction studies of complex **10** confirmed the distorted T-shaped geometry around its platinum centre (Fig. 3) – a common feature of MOLPs involving $[PtL_2]$ Lewis bases.[39–46] The Pt–Sn bond of this dicationic complex is even shorter than that of the monocationic complex (**10**: 2.502(1) Å; **7b**: 2.524(1) Å). The tin center is weakly coordinated by three bromide atoms of two aluminate counteranions, with a $Sn\cdots Br(WCA)_{avg}$ distance of 3.055(5) Å, markedly shorter than the sum of their van der Waals radii (4.0 Å).[56] The shortest Sn–Br distance in **10** (2.956(1) Å) is significantly longer than regular Sn–Br bond lengths (*ca.* 2.59 Å).[57] The published arene-stabilized, chlorine-bridged tin monocations $[\eta^6\text{-}(C_6H_6)_2SnCl(AlCl_4)]_2$ (**12**),[58] and $[\eta^6\text{-}(C_6Me_6)SnCl(AlCl_4)]_4$ (**13**)[59] also possess bonds that are shorter than sum of their van der Waals radii (3.496(2) Å *vs.* 3.92 Å).[56,57]

Similar structural features are also observed in the case of **11** (Fig. 3), which exhibits a distorted T-shaped geometry around its platinum centre. The Pt–Pb bond length of **11** (2.564(1) Å) is 0.04 Å shorter than that in **8a** and is shorter than typical Pt–Pb bonds. For example, the Pt–Pb distances in the metallocryptate $[Pt_2(P_2phen)_3Pb][ClO_4]_2$ are 2.747(1) and 2.733(1) Å, indicating an attractive metallophilic interaction rather than Lewis acid–base interactions.[26] The Pt–Pb distance in the complex $[(AcO)Pb(crown\text{-}P_2)Pt(CN)_2][(O_2CCH_3)]$ (**H**) (3.313(2) Å) is long enough to raise questions about the existence of bonding between these two entities.[27] Another Pt–Pb compound, $[nBu_4N]_2[\{Pt(C_6F_5)_4\}_2(Pb)]$ (**I**), shows interactions between the Pb center and the *endo* fluorine atoms.[28] The Pb center in **11** also exhibits weak interactions with two aluminate anions ($Pb\cdots Cl(WCA)_{avg}$ 3.001(1) Å), leading to a pseudo-T-shaped geometry at the Pb atom.[56] We cannot disregard two additional Pb···Cl interactions with the $[AlCl_4]^-$ anions (3.592(1) Å), which although long are nevertheless

 

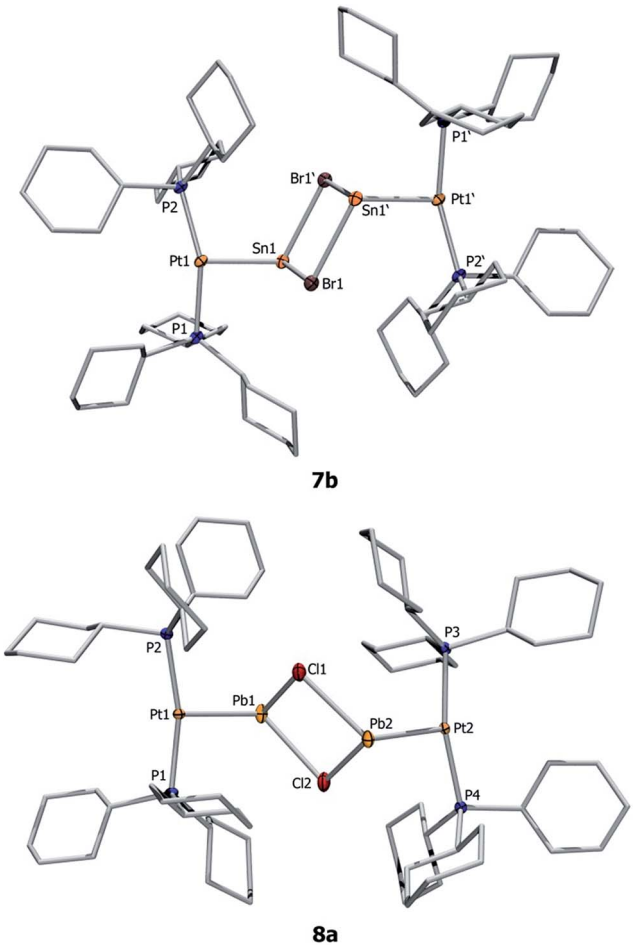


Fig. 2 Molecular structures of **7b** and **8a**. Ellipsoids are drawn at the 50% probability level. Hydrogen atoms, counteranions (two $[AlCl_4]^-$ or $[BAr^{Cl}{}_4]^-$ units), and ellipsoids of the cyclohexyl rings are omitted for clarity. Selected bond lengths [Å] and angles [°], calculated values are in parentheses: **7b**: Pt1–Sn1 2.524(1), Sn1–Br1 2.780(1), Sn1–Br1′ 2.821(1), P1–Pt–P2 159.9(1), Br1–Sn1–Br1′ 84.1(1), Pt1–Sn1–Br1 93.9(1), Pt1–Sn1–Br1′ 114.0(1); **8a**: Pt1–Pb1 2.603(1) (2.626), Pb1–Cl1 2.763(4) (2.720), Pb1–Cl2 2.829(3) (2.777), Pt2–Pb2 2.603(2) (2.622), Pb2–Cl2 2.719(4) (2.724), Pb2–Cl1 2.766(4) (2.786), Pb1···Cl(WCA) 3.420(1); P2–Pt1–P1 162.56(10) (159.9), Cl1–Pb1–Cl2 77.32(10) (80.4), P3–Pt2–Pb2–Cl2 112.28(10) (104.6).

shorter than the sum of the van der Waals radii (3.77 Å).[56] Our calculations also showed that these interactions persist even in the gas phase, provided non-constrained calculations were used. The Pb···Cl interaction is considerably shorter than those in **8a** (3.420(1) Å) but significantly longer than the Pb–Cl single bond length (2.300(4) Å) reported for LPbCl [L = HC(CMeNAr)$_2$ (Ar = 2,6-i$Pr_2C_6H_3$)] (**14**).[60] The distance is in the same range as other weak Pb···Cl interactions, *e.g.* in the arene-stabilized lead(II) dications [(1,2-$C_6H_4Me_2$)$_2$Pb ($AlCl_4$)$_2$] (**F**) (2.969(1) Å) or [($C_6H_6$)$_2$Pb][$AlCl_4$]$_2$ (**15**) (2.854(8)–3.218(9) Å).[20,22]

We subsequently attempted exchange of the donor fragment [($Cy_3P$)$_2$Pt] from the dication **11**. Upon addition of aromatic donor ligands (benzene and fluorobenzene), no exchange reaction was observed. Likewise, no exchange was observed upon addition of the strong N-donor ligand DMAP.

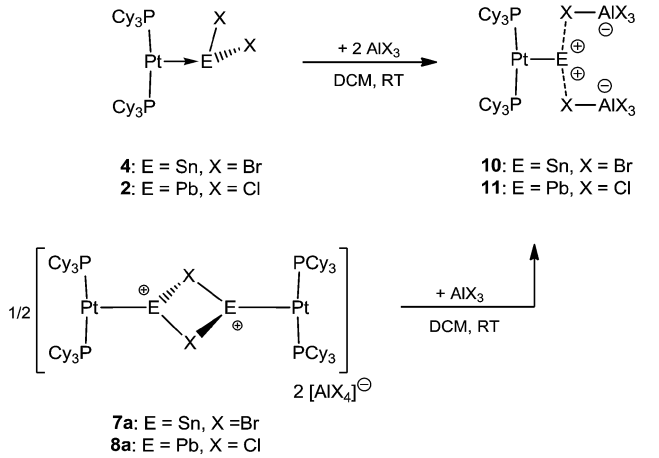


Scheme 4 Formation of the pseudo-monocoordinate dications of tin (**10**) and lead (**11**).

## Synthesis of a stannyl anion

After the isolation of low-valent tin mono- and dications by halide abstraction from **4**, we sought to conversely add another halide to form anionic tin compounds. The preparation of the anionic species [N*n*$Bu_4$][($Cy_3P$)$_2$Pt($SnBr_3$)] (**16**) is shown in Scheme 5.

The stoichiometric addition of [N*n*$Bu_4$]Br to **4** resulted in the formation of an anionic complex containing a formal Pt–Sn dative bond, along with a tetrabutylammonium countercation, [N*n*$Bu_4$][($Cy_3P$)$_2$Pt($SnBr_3$)] (**16**), in good yields (80%). Such additions of bromide anions to tin(II) compounds, yielding anionic tin(II) salts, are known in cases where the tin atom is ligated by main group donors, but are unknown in cases where the Lewis base is a transition metal fragment.[61,62] The $^{31}P\{^1H\}$ NMR spectra of **16** reveals a sharp singlet at $\delta$ = 56.2 ppm ($^1J_{P-Pt}$ = 4634 Hz), slightly upfield in comparison to that of precursor **4** $\delta$ = 49.7 ppm ($^1J_{P-Pt}$ = 3421 Hz), while the coupling constant increased by ~1200 Hz, indicating a significantly modified chemical environment around the Sn atom. As in previous cases, all attempts to detect $^{119}Sn\{^1H\}$ NMR resonances failed.[49,50]

Red crystals of **16** were analyzed by single-crystal X-ray diffraction (Fig. 4), displaying a Pt–Sn distance (2.604(1) Å) nearly identical to that of its precursor (2.605(2) Å). As expected, the Sn atom is strongly pyramidalized. The average Sn–Br distance in the stannyl anion (2.69 Å) is longer than the average Sn–Br distance (2.63 Å) in **4**, presumably due to the introduction of another Br, which increases the steric demand at the Sn center.

## Reactivity of low-valent Pb cations

Cationic species are known to form adducts with Lewis bases,[3] prompting us to study the reaction of **8a** with 4-picoline. This reaction afforded the 4-picoline-coordinated low-valent Pb cation [{($Cy_3P$)$_2$Pt}PbCl(4-pic)][$AlCl_4$] (**17**) (Scheme 6). Although all attempts to grow X-ray quality single crystals for diffraction analysis failed, the formation of **17** was clearly demonstrated

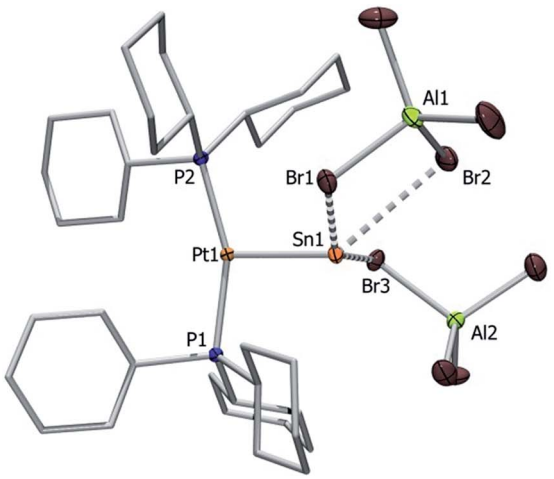


**10**

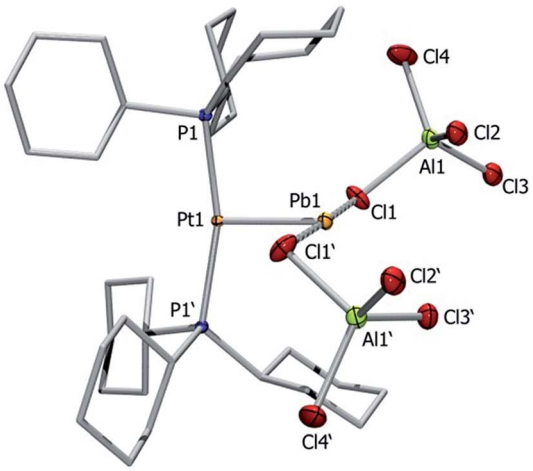


**11**

Fig. 3 Molecular structures of **10** and **11**. Thermal ellipsoids are drawn at the 50% probability level. Hydrogen atoms and ellipsoids of the cyclohexyl rings are omitted for clarity. Selected bond lengths [Å] and angles [°]: **10**: Pt1–Sn1 2.502(1), Sn1–Br1 3.155(1), Sn1–Br2 3.264 (1), Sn1–Br3 2.956(1), P1–Pt–P2 158.0(1), P1–Pt1–Sn1 93.6(1), P2–Pt1–Sn1 106.7(1); **11**: Pt1–Pb1 2.564(1), Pb1···Cl(WCA) 3.001(1); P1′–Pt1–P1 162.23(4), Cl1–Pb1–Cl1′ 177.90(4), P1–Pt1–Pb1–Cl1 −77.65(3), Pt1–Pb1–Cl1–Al1 143.81(4).

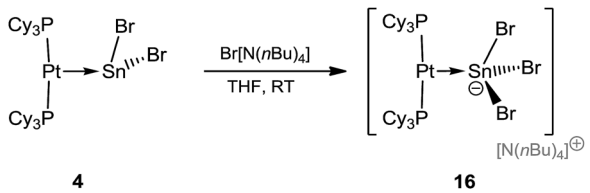


**4** **16**

Scheme 5 Formation of the anionic complex **16**.

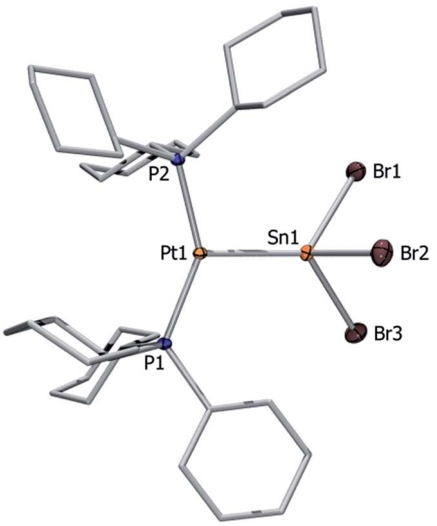


Fig. 4 Molecular structure of the anion of **16**. Ellipsoids are drawn at the 50% probability level. Hydrogen atoms, countercations ($[nBu_4N]^+$), solvent molecules and ellipsoids of the cyclohexyl rings are omitted for clarity. Selected bond lengths [Å] and angles [°]: Pt1–Sn1 2.604(1), Sn1–Br1 2.698(2), Sn1–Br2 2.675(2), Sn1–Br3 2.718(1), P1–Pt–P2 145.1(1), P1–Pt1–Sn1 111.4(2), P2–Pt1–Sn1 102.3(1).

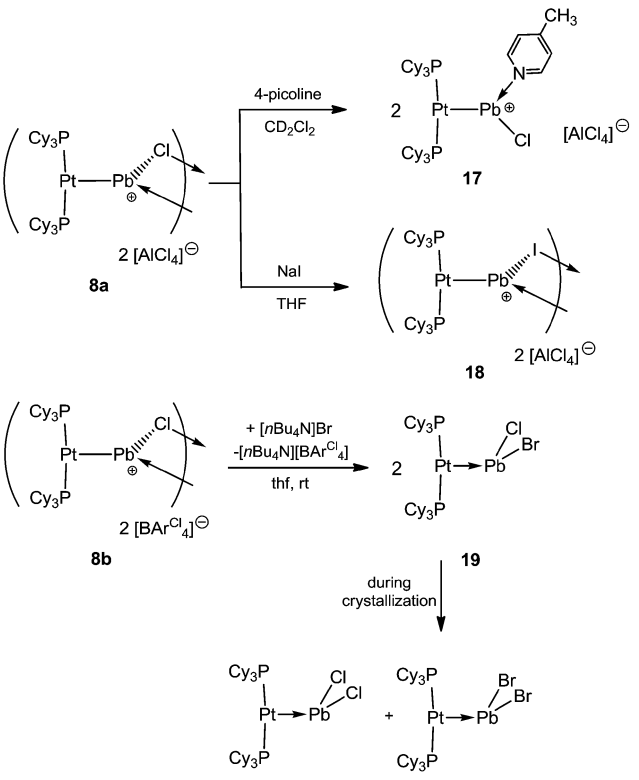


Scheme 6 Reactivity of the new cationic PtPb complexes.

from its $^{31}P\{^1H\}$ NMR spectrum (**17**: $\delta = 47.1$ ppm; $^1J_{P-Pt} = 3370$ Hz), which showed an increase of the coupling constant with respect to that of the starting material (**8a**: $\delta = 46.6$ ($^1J_{P-Pt} = 3100$ Hz) ppm). Additionally, we were able to see the respective picoline resonances, with appropriate integration, in the $^1H$ and $^{13}C\{^1H\}$ NMR spectra, slightly shifted with respect to free picoline.

To further investigate the reactivity of our cationic plumbylene complexes we attempted halide exchange reactions.

Addition of NaI to a THF solution of **8a** led to a halide exchange reaction at the Pb atoms and isolation of the new dinuclear dicationic complex $[(Cy_3P)_2Pt(PbI)]_2[AlCl_4]_2$ (**18**) (Scheme 6). The $^{31}P\{^1H\}$ NMR spectrum of **18** reveals a sharp singlet at $\delta = 45.5$ ppm ($^1J_{P-Pt} = 3130$ Hz). Single crystal X-ray determination showed the same constitution as compound **8a**. The Pt–Pb and Pb–I bond lengths in **18** are 2.61(1) Å and 2.917(1)/3.092(1) Å, respectively (see ESI†). All bond lengths are slightly elongated with respect to the chloro precursor **8a**, as expected due to the larger covalent radius of iodide.[56]

In contrast to **8a**, the reaction between **8b** and $[NnBu_4]Br$ in THF resulted in a MOLP containing a lead atom with mixed halogens $[(Cy_3P)_2Pt–PbClBr]$ (**19**) instead of a putative halogen exchange product (Scheme 6). Despite the absence of structural evidence, the formation of **19** was apparent from the $^{31}P\{^1H\}$ and $^{195}Pt\{^1H\}$ NMR spectra, which show a singlet at $\delta = 48.6$ ppm ($^1J_{P-Pt} = 3520$ Hz) and a triplet at $\delta = -3950$ ppm, respectively. These data show very little difference to those of the dichloro analogue **2** ($^{31}P$: $\delta = 48.3$ ($^1J_{Pt-P} = 3450$ Hz) ppm, $^{195}Pt$: $\delta = -4025$ ppm). During crystallization from toluene, a disproportionative halide exchange takes place, leading to the formation of two neutral species, $[(Cy_3P)_2Pt–PbX_2]$ (X = Cl, Br), which were confirmed by X-ray structure analysis as well as by $^{31}P\{^1H\}$ NMR spectroscopy. This serendipitous finding serves as further evidence for the formation of complex **19**.

### DFT calculations on the PtPb complexes 2, 8a and 11

In order to gain a deeper understanding of the bonding situation in the PtPb complexes **2**, **8a** and **11**, quantum chemical calculations were carried out at the RI-D3(BJ)-BP86 level using def2-TZVP for the non-metal atoms and def2-QZVP for the Pt and Pb atoms.[63–67] The optimized geometries of the complexes are shown in Fig. 5, including the most important bond lengths and bond angles. The calculated bond lengths agree well with the experimental bond lengths when the intermolecular dispersion interactions, and especially the damping factor (BJ), have been taken into account, as its importance has been previously reported by Grimme.[68] A constrained geometry optimization was performed for **11** to further analyze the Pt–Pb bond because its non-constrained optimization converged to a structure in which two chloride atoms Cl2 and Cl2′ are bound to Pb1 (**11a**, Fig. 5). This is presumably a result of the absence of crystal packing effects, as the chloride atoms are presumably stabilized by the dielectric field created by the positively charged protons on the cyclohexyl groups of the surrounding molecules. We discuss the interaction of Cl2 and Cl2′ with Pb1 in detail in the bond analysis section below.

NBO analysis[69] shows that the Pt atom always carries a negative charge in these complexes (−0.483, −0.420 and −0.485*e* in **2**, **8a** and **11**, respectively), which means there is a significant charge donation from the ligands to Pt, especially from the strong $PCy_3$ donor ligands. However, the partial charges of the Pb atoms are always positive (1.174, 1.124 and 1.070*e* in **2**, **8a** and **11**, respectively), and remain relatively constant upon successive halide abstraction and increase of net positive charge. This suggests that build-up of positive charge

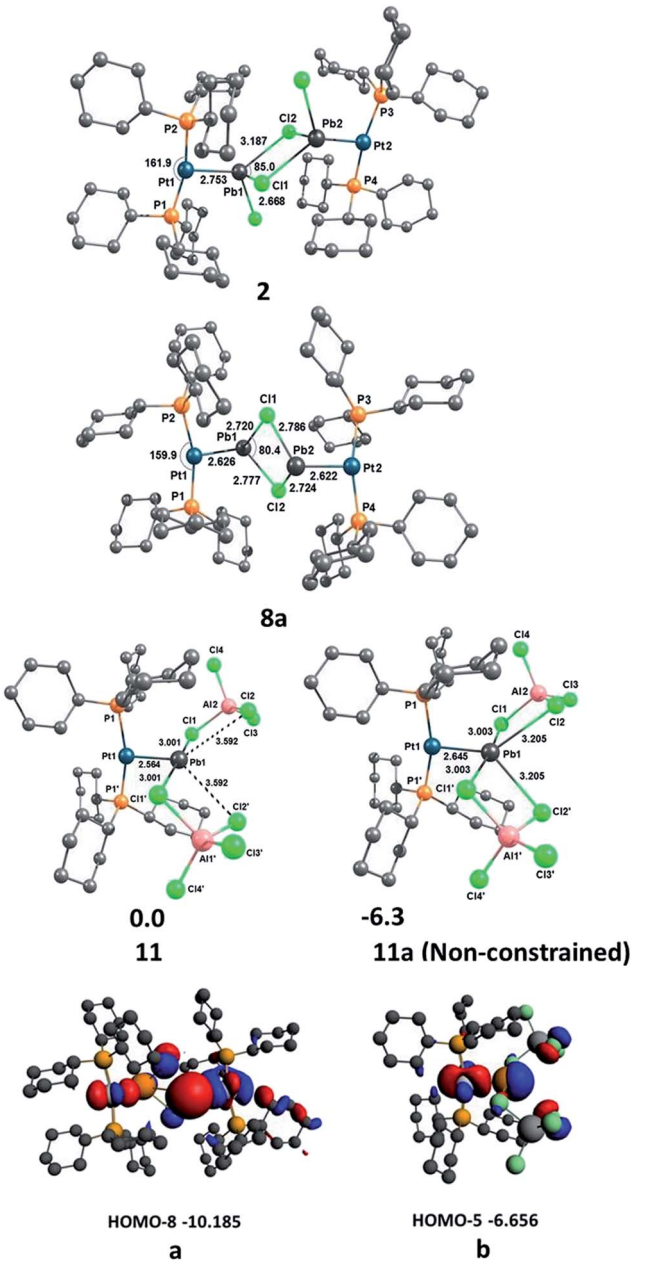


Fig. 5 Above: optimized geometries of **2**, **8a**, **11** and **11a** at the RI-D3(BJ)-BP86/def2-TZVP + def2-QZVP level. Bond lengths are given in Å, angles in (°) and energies in kcal $mol^{-1}$; below: plot of (a) HOMO-8 of **8a** and (b) HOMO-5 of **11** (eV) at the D3(BJ) + BP86/TZ2P//RI-D3(BJ)-BP86/def2-TZVP + def2-QZVP level.

created by the removal of halides from Pb is effectively compensated by the connected groups, which, given the relatively constant charge on Pt, presumably stems from the short contacts with nearby halides.

We investigated the nature of the Pt–Pb bonding in the complexes **2**, **8a** and **11** with an energy decomposition analysis (EDA-NOCV)[70] using two different fragmentation patterns, D and E. D describes donor–acceptor interactions whereas E describes an electron sharing bonding scheme between the Pt and Pb fragments. The EDA-NOCV data given in Table 2 suggest

Table 2 EDA-NOCV results of the analysis of Pt–Pb bonds in **2**, **8a** and **11** at the D3(BJ) + BP86/TZ2P//RI-D3(BJ)-BP86/def2-TZVP + def2-QZVP level (kcal mol$^{-1}$)

| Compound | **2** | **2** | **8a** | **8a** | **11** | **11** |
|---|---|---|---|---|---|---|
| Fragmentation pattern | D[c] | E[c] | D[c] | E[c] | D[c] | E[c] |
| Fragment 1 | $[(Cy_3P)_2Pt]$ | $[Cy_3P]_2Pt^+$ | $[(Cy_3P)_2Pt]$ | $[(Cy_3P)_2Pt]^+$ | $[(Cy_3P)_2Pt]$ | $[(Cy_3P)_2Pt]^+$ |
| Fragment 2 | $[PbCl_2–PbCl_2–Pt(PCy_3)_2]$ | $[PbCl_2–PbCl_2–Pt(PCy_3)_2]^-$ | $[PbCl–PbCl–Pt(PCy_3)_2]^{2+}$ | $[PbCl–PbCl–Pt(PCy_3)_2]^+$ | $[Cl_4Al–Pb–AlCl_4]$ | $[Cl_4Al–Pb–AlCl_4]^-$ |
| $\Delta E_{int}$ | −68.3 | −176.0 | −128.1 | −77.1 | −120.5 | −163.9 |
| $\Delta E_{Pauli}$ | 146.9 | 169.5 | 173.7 | 192.9 | 200.5 | 249.7 |
| $\Delta E_{elstat}$[a] | −104.7 (48.7%) | −183.1 (53.0%) | −124.2 (41.2%) | −112.7 (41.7%) | −139.9 (43.6%) | −246.5 (59.6%) |
| $\Delta E_{disp}$[a] | −44.7 (20.8%) | −44.7 (12.9%) | −50.1 (16.6%) | −50.1 (18.5%) | −49.8 (15.5%) | −49.8 (12.0%) |
| $\Delta E_{orb}$[a] | −65.7 (30.5%) | −117.7 (34.1%) | −127.5 (42.2%) | −107.3 (39.7%) | −131.4 (40.9%) | −117.4 (28.4%) |
| $\Delta E_\sigma$[b] Pt → Pb | −32.6 (49.6%) | — | −65.1 (51.1%) | — | −60.2 (45.8%) | — |
| $\Delta E_\sigma$[b] Pt–Pb | — | −87.2 (74.1%) | — | −67.5 (62.9%) | — | −70.1 (59.7%) |
| $\Delta E_{\pi\parallel}$[b] Pt → Pb | −7.1 (10.8%) | −2.4 (2.0%) | −9.7 (7.6%) | −10.6 (9.9%) | −9.7 (7.4%) | −17.2 (14.7%) |
| $\Delta E_{\pi\perp}$[b] Pt → Pb | −4.8 (7.3%) | −4.8 (4.1%) | −15.4 (12.1%) | −6.2 (5.8%) | −25.4 (19.3%) | −6.4 (5.5%) |
| $\Delta E_\sigma$[b] Pb → Pt | −3.8 (5.8%) | — | −5.3 (4.2%) | — | −4.0 (3.0%) | — |
| Rest[b] | −17.4 (26.5%) | −23.3 (19.8%) | −32.0 (25.0%) | −23.0 (21.4%) | −32.1 (24.5%) | −23.6 (20.2%) |
| $\Delta E_{prep}$ | 12.9 | 5.1 | 37.5 | 17.3 | 52.9 | 12.3 |
| $-D_e$ | −55.4 | −170.9 | −90.6 | −59.8 | −67.6 | −151.6 |

[a] The values in parentheses give the percentage contribution to the total attractive interactions $\Delta E_{elstat} + \Delta E_{disp} + \Delta E_{orb}$. [b] The values in parentheses give the percentage contribution to the total orbital interactions $\Delta E_{orb}$. [c] D: donor–acceptor bonding model; E: electron sharing bonding model.

that the Pt–Pb bond in **2** is dative in nature, whereas those of **8a** and **11** are electron-sharing bonds. The $\Delta E_{orb}$ value of **2** in model D (−65.7 kcal mol$^{-1}$), where both the singlet state of $[(Cy_3P)_2Pt]$ and $[PbCl_2–PbCl_2–Pt(PCy_3)_2]$ were used as interacting fragments, has a weaker interaction than model E ($\Delta E_{orb}$ = −117.7 kcal mol$^{-1}$), where doublet states of $[(Cy_3P)_2Pt]^+$ and $[PbCl_2–PbCl_2–Pt(PCy_3)_2]^-$ were used as interacting fragments. Here we applied the rule that the best description of a chemical bond comes from the interacting fragments that give the weakest orbital interaction ($\Delta E_{orb}$), as suggested by Frenking based on his work on carbodiphosphoranes in which the same charge and spin states of the fragments were compared,[71] in addition to his other work in which different charge and spin states of the fragments were compared for the analysis of M–E (M = Fe, Ru, Os; E = C–Sn)[72] and E–C bonds (E = Be, $B^+$, $C^{2+}$, $N^{3+}$, $O^{4+}$).[73] The $\Delta E_{orb}$ values of **8a** (−107.3 kcal mol$^{-1}$) and **11** (−117.4 kcal mol$^{-1}$) in model E are significantly lower than those of **8a** (−127.5 kcal mol$^{-1}$) and **11** (−131.4 kcal mol$^{-1}$) in model D. Therefore, the Pt–Pb bonds in **8a** and **11** are electron-sharing in nature, whereas that of **2** is a dative bond. This difference in bonding upon halide abstraction suggests that the electron pair donated by Pt to Pb in **2** is converted to a fully-covalent bonding σ orbital in **8a** and **11**. The analysis of the Kohn–Sham molecular orbitals reveals that the HOMO-8 of **8a** (a, Fig. 5) and HOMO-5 of **11** (b, Fig. 5) both exhibit σ orbitals formed from a d orbital of Pt and a p orbital of Pb.

We have analyzed the Pb–Cl bonding in **2**, **8a** and **11** with the EDA-NOCV method using singlet $[(Cy_3P)_2Pt–PbCl_2]$ for **2**, singlet $[(Cy_3P)_2Pt–PbCl]^+$ for **8a** and singlet $[(Cy_3P)_2Pt–Pb]^{2+}$ and $[AlCl_4\cdots AlCl_4]^{2-}$ for **11** as interacting fragments. The EDA-NOCV results (Table 3) show that the orbital (covalent) interactions $\Delta E_{orb}$ are stronger (−67.7 kcal mol$^{-1}$) than the electrostatic (ionic) interactions $\Delta E_{elstat}$ (−48.7 kcal mol$^{-1}$) in **8a**. However, the electrostatic interactions are stronger in **2** (−43.0 kcal mol$^{-1}$) and **11** (−257.6 kcal mol$^{-1}$) than the corresponding orbital interactions in **2** (−26.6 kcal mol$^{-1}$) and **11** (−69.9 kcal mol$^{-1}$) (Table 3). The breakdown of $\Delta E_{orb}$ into contributions from orbitals having different symmetry reveals that the dominant contribution comes from Cl → Pb σ-donation. The Pb → Cl σ backdonation is very weak for **8a** (11.1%) and almost negligible for **2** (4.9%) and **11** (1.7%). The crystal structure of **11** shows two additional Pb1⋯Cl2 and Pb1⋯Cl2′ short contacts (3.592 Å) and non-constrained gas phase optimization (**11a**, Fig. 5) converged to a structure in which these short contacts strengthen (3.205 Å), the structure thereby becoming similar to the structure of $[(1,2\text{-}C_6H_4Me_2)_2Pb][AlCl_4]_2$ (**F**) reported by Frank *et al.*[22] According to the EDA-NOCV method, the sum of the orbital interaction energies of the two Pb1⋯Cl2 and Pb1⋯Cl2′ contacts is very weak (11.9 kcal mol$^{-1}$), indicating that each of these contacts has a roughly 6.0 kcal mol$^{-1}$ orbital interaction energy. These two chloride atoms in the crystal are presumably stabilized by the positively charged protons on the cyclohexyl groups of the surrounding molecules. In the absence of crystal packing effects, Pb1⋯Cl2 and Pb1⋯Cl2′ interactions strengthen and the non-constrained gas phase optimized geometry **11a** becomes similar to the aforementioned structure reported by Frank *et al.* The bond dissociation energies decrease to −4.7 kcal mol$^{-1}$ for **2** and +25.3 kcal mol$^{-1}$ for **8a** without including dispersion energies, which shows the importance of introducing the dispersion interactions.[68] It is clear that

 

Table 3 EDA-NOCV results of the analysis of Pb–Cl bonding in **2**, **8a** and **11** at the D3(BJ) + BP86/TZ2P//RI-D3(BJ)-BP86/def2-TZVP + def2-QZVP level (kcal mol$^{-1}$)

| Compound | **2** | **8a** | **11** |
|---|---|---|---|
| Fragment 1 | $[(Cy_3P)_2Pt–PbCl_2]$ | $[(Cy_3P)_2Pt–PbCl]^+$ | $[(Cy_3P)_2Pt–Pb]^{2+}$ |
| Fragment 2 | $[(Cy_3P)_2Pt–PbCl_2]$ | $[(Cy_3P)_2Pt–PbCl]^+$ | $[AlCl_4\cdots AlCl_4]^{2-}$ |
| $\Delta E_{int}$ | −40.5 | −29.9 | −290.2 |
| $\Delta E_{Pauli}$ | 61.1 | 129.7 | 76.3 |
| $\Delta E_{elstat}$ [a] | −43.0 (42.3%) | −48.7 (30.5%) | −257.6 (70.3%) |
| $\Delta E_{disp}$ [a] | −32.0 (31.5%) | −43.2 (27.1%) | −39.1 (10.7%) |
| $\Delta E_{orb}$ [a] | −26.6 (26.2%) | −67.7 (42.4%) | −69.9 (19.0%) |
| $\Delta E_{\sigma}$ [b] Cl → Pb | −13.6 (51.1%) | −39.1 (57.8%) | −25.8 (36.9%) |
| $\Delta E_{\sigma}$ [b] Pb → Cl | −1.3 (4.9%) | −7.5 (11.1%) | 1.2 (1.7%) |
| $\Delta E_{\pi\perp}$ [b] Cl → Pb | −1.5 (5.6%) | −7.1 (10.5%) | 2.0 (2.9%) |
| $\Delta E_{\sigma}$ [b] (Cl2, Cl6) → Pb | — | — | −11.9 (17.0%) |
| Rest [b] | −10.2 (38.3%) | −14.0 (20.7%) | −29.0 (41.5%) |
| $\Delta E_{prep}$ | 3.8 | 12.0 | 50.4 |
| $-D_e$ | −36.7 | −17.9 | −239.8 |

[a] The values in parentheses give the percentage contribution to the total attractive interactions $\Delta E_{elstat} + \Delta E_{disp} + \Delta E_{orb}$. [b] The values in parentheses give the percentage contribution to the total orbital interactions $\Delta E_{orb}$.

dispersion interactions have a strong effect on the thermodynamic stability of **2** and **8a**, as mentioned in the analysis of the Pt–Pb bonds above, as was also pointed out by Power *et al.*[74]

## Conclusions

In this paper, we have sequentially abstracted halide ions from dihalostannylene and plumbylene complexes, leading first to dicationic dinuclear complexes and then to unprecedented low-valent dicationic complexes containing Pt–Sn and Pt–Pb bonds. The reactivity of a number of the neutral and cationic complexes with halide salts and Lewis bases was also probed. The EDA-NOCV data reveal that the Pt–Pb bond is electron-sharing in nature in **8a** and **11**, whereas it is a dative bond in **2**. The EDA-NOCV data also reveal that the ionic interactions in Pt–Pb bond are always stronger than the covalent interactions in **2**, **8a** and **11**. Ionic interactions also predominate in the Pb–Cl bonds of **2** and **11**, but not **8a**. The calculated D3 intramolecular dispersion energies in the analysis of Pt–Pb and Pb–Cl bonds indicate that dispersion forces have an important effect on the thermodynamic stability of **2**, **8a** and **11**.

## Computational details

Geometry optimizations of the complexes were carried out at BP86 [66] level using a mix basis set of def2-TZVP[67] for nonmetals and def2-QZVP[67] for Pt and Pb, as implemented in Turbomole 6.5.[75] DFT-D3 [64] was used to include van der Waals forces including the Becke–Johnson damping (BJ).[65] The geometry optimizations were performed without geometry constraints for **2**, **8a** and **11a**. However, a constrained geometry optimization has also been performed for **11** where P1, P1′, Pt1, Pb1, Cl1, Cl2, Cl4, Cl1′, Cl2′ and Cl4′ (Fig. 5) were frozen to their X-ray structure positions, as the non-constrained geometry optimization converged to a structure (**11a**) in which two chloride atoms were bound to the Pb1 atom. The NBO[69] charges were calculated at the same level of theory. All complexes were characterized as minima by calculation of vibrational frequencies. The resolution-of-identity (RI)[63] method was used for the calculations.

The calculations for the energy decomposition analysis (EDA-NOCV)[70] were carried out with the program package ADF 2013.01 [76] at BP86 in conjunction with a triple-ζ-quality basis set TZ2P[77] where relativistic effects are considered with the ZORA approximation.[78] The RI-D3(BJ)-BP86/def2-TZVP + def2-QZVP optimized geometries were used for the EDA-NOCV calculations. The effect of dispersion interactions on EDA-NOCV were estimated using the D3 dispersion correction including BJ damping. This level of theory is denoted D3(BJ) + BP86/TZ2P//RI-D3(BJ)-BP86/def2-TZVP + def2-QZVP. In the EDA the bond dissociation energy, $D_e$, of a molecule (AB) is divided into the preparation energy $\Delta E_{prep}$ and the intrinsic interaction energy $\Delta E_{int}$:

$$\Delta E\,(=-D_e) = \Delta E_{int} + \Delta E_{prep} \quad (1)$$

The intrinsic interaction energy $\Delta E_{int}$ is further divided into four main components:

$$\Delta E_{int} = \Delta E_{elstat} + \Delta E_{disp} + \Delta E_{Pauli} + \Delta E_{orb} \quad (2)$$

The $\Delta E_{elstat}$ parameter corresponds to the quasiclassical electrostatic interaction energy between the fragments calculated by means of the frozen electron density distribution of the fragments in the geometry of the molecules. $\Delta E_{disp}$ accounts for the intramolecular dispersion energy. $\Delta E_{Pauli}$ refers to the repulsive interactions between the fragments, which include destabilizing interactions between occupied orbitals and any steric repulsion. The stabilizing orbital interaction term $\Delta E_{orb}$ is calculated in the final step of the energy partitioning analysis when the Kohn–Sham orbitals relax to their optimal form.

## Acknowledgements

This work was supported by the Deutsche Forschungsgemeinschaft. SSS thanks the AvH foundation for a postdoctoral fellowship.

## Notes and references

1 P. Jutzi, F. Kohl, P. Hofmann, C. Krueger and Y.-H. Tsay, *Chem. Ber.*, 1980, **113**, 757.
2 P. A. Rupar, V. N. Staroverov and K. M. Baines, *Science*, 2008, **322**, 1360.
3 S. Khan, G. Gopakumar, W. Thiel and M. Alcarazo, *Angew. Chem., Int. Ed.*, 2013, **52**, 5644.
4 M. Driess, S. Yao, M. Brym and C. van Wullen, *Angew. Chem., Int. Ed.*, 2006, **45**, 6730.
5 B. Rhodes, J. C. W. Chien and M. D. Rausch, *Organometallics*, 1998, **17**, 1931.
6 T. Probst, O. Steigelmann, J. Riede and H. Schmidbaur, *Angew. Chem., Int. Ed. Engl.*, 1990, **29**, 1397.
7 J. Li, C. Schenk, F. Winter, H. Scherer, N. Trapp, A. Higelin, S. Keller, R. Pottgen, I. Krossing and C. Jones, *Angew. Chem., Int. Ed.*, 2012, **51**, 9557.
8 A. Schäfer, F. Winter, W. Saak, D. Haase, R. Pöttgen and T. Müller, *Chem.–Eur. J.*, 2011, **17**, 10979.
9 T. Müller, *Adv. Organomet. Chem.*, 2005, **53**, 155.
10 P. A. Rupar, V. N. Staroverov, P. J. Ragogna and K. M. Baines, *J. Am. Chem. Soc.*, 2007, **129**, 15138.
11 P. A. Rupar, R. Bandyopadhyay, B. F. T. Cooper, M. R. Stinchcombe, P. J. Ragogna, C. L. B. Macdonald and K. M. Baines, *Angew. Chem., Int. Ed.*, 2009, **48**, 5155.
12 F. Cheng, A. L. Hector, W. Levason, G. Reid, M. Webster and W. Zhang, *Angew. Chem., Int. Ed.*, 2009, **48**, 5152.
13 P. Jutzi, A. Mix, B. Rummel, W. W. Schoeller, B. Neumann and H. G. Stammler, *Science*, 2004, **305**, 849.
14 P. Jutzi, R. Dickbreder and H. Nöth, *Chem. Ber.*, 1989, **122**, 865.
15 S. Hino, M. Brynda, A. D. Phillips and P. P. Power, *Angew. Chem., Int. Ed.*, 2004, **43**, 2655.
16 M. J. Taylor, A. J. Saunders, M. P. Coles and J. R. Fulton, *Organometallics*, 2011, **30**, 1334.
17 A. M. Orlova, I. B. Sivaev, V. L. Lagun, S. B. Katser, K. A. Solntsev and N. T. Kuznetsov, *Russ. J. Coord. Chem.*, 1996, **22**, 110.
18 J. M. Harrowfield, H. Miyamae, B. W. Skelton, A. A. Soudi and A. H. White, *Aust. J. Chem.*, 2002, **55**, 661.
19 M. Kadarkaraisamy, D. P. Engelhart, P. N. Basa and A. G. Sykes, *J. Coord. Chem.*, 2010, **63**, 2261.
20 A. G. Gash, P. F. Rodesiler and E. L. Amma, *Inorg. Chem.*, 1974, **13**, 2429.
21 V. N. Kokozay and A. V. Sienkiewicz, *Polyhedron*, 1995, **14**, 1547.
22 W. Frank and F. G. Wittmer, *Chem. Ber.*, 1997, **130**, 1731.
23 A. C. Filippou, P. Portius and A. I. Philippopoulos, *Organometallics*, 2002, **21**, 653.
24 A. C. Filippou, A. I. Philippopoulos and G. Schnakenburg, *Organometallics*, 2003, **22**, 3339.
25 A. C. Filippou, A. I. Philippopoulos, P. Portius and G. Schnakenburg, *Organometallics*, 2004, **23**, 4503.
26 V. J. Catalano, B. L. Bennett and B. C. Noll, *Chem. Commun.*, 2000, 1413.
27 A. L. Balch, E. Y. Fung, J. K. Nagle, M. M. Olmstead and S. P. Rowley, *Inorg. Chem.*, 1993, **32**, 3295.
28 R. Uson, J. Fornies, L. R. Falvello, M. A. Uson and I. Uson, *Inorg. Chem.*, 1992, **31**, 3697.
29 H. Braunschweig, A. Damme, R. D. Dewhurst and A. Vargas, *Nat. Chem.*, 2013, **5**, 115.
30 H. Braunschweig, K. Radacki and K. Uttinger, *Angew. Chem., Int. Ed.*, 2007, **46**, 3979.
31 H. Braunschweig, K. Radacki, D. Rais and D. Scheschkewitz, *Angew. Chem., Int. Ed.*, 2005, **44**, 5651.
32 H. Braunschweig, K. Radacki and K. Uttinger, *Organometallics*, 2008, **27**, 6005.
33 H. Braunschweig, P. Brenner, R. D. Dewhurst, J. O. C. Jimenez-Halla, T. Kupfer, D. Rais and K. Uttinger, *Angew. Chem., Int. Ed.*, 2013, **52**, 2981.
34 H. Braunschweig, K. Radacki, D. Rais and K. Uttinger, *Angew. Chem., Int. Ed.*, 2006, **45**, 162.
35 H. Braunschweig, T. Kupfer, K. Radacki, A. Schneider, F. Seeler, K. Uttinger and H. Wu, *J. Am. Chem. Soc.*, 2008, **130**, 7974.
36 H. Braunschweig, K. Radacki and A. Schneider, *Science*, 2010, **328**, 345.
37 J. Brand, H. Braunschweig and S. S. Sen, *Acc. Chem. Res.*, 2014, **47**, 180.
38 J. Brand, H. Braunschweig, F. Hupp, A. K. Phukan, K. Radacki and S. S. Sen, *Angew. Chem., Int. Ed.*, 2014, **53**, 2240.
39 H. Braunschweig, K. Gruss and K. Radacki, *Angew. Chem., Int. Ed.*, 2009, **48**, 4239.
40 H. Braunschweig, K. Gruss and K. Radacki, *Angew. Chem., Int. Ed.*, 2007, **46**, 7782.
41 H. Braunschweig, K. Gruss and K. Radacki, *Inorg. Chem.*, 2008, **47**, 8595.
42 H. Braunschweig, P. Brenner, P. Cogswell, K. Kraft and K. Schwab, *Chem. Commun.*, 2010, **46**, 7894.
43 H. Braunschweig, K. Radacki and K. Schwab, *Chem. Commun.*, 2010, **46**, 913.
44 H. Braunschweig, P. Cogswell and K. Schwab, *Coord. Chem. Rev.*, 2011, **255**, 101.
45 J. Bauer, H. Braunschweig, P. Brenner, K. Kraft, K. Radacki and K. Schwab, *Chem.–Eur. J.*, 2010, **16**, 11985.
46 J. Bauer, H. Braunschweig and R. D. Dewhurst, *Chem. Rev.*, 2012, **112**, 4329.
47 H. Braunschweig, A. Damme, R. D. Dewhurst, F. Hupp, J. O. C. Jimenez-Halla and K. Radacki, *Chem. Commun.*, 2012, **48**, 10410.
48 W. H. Liao, P. Y. Ho and M. D. Su, *Inorg. Chem.*, 2013, **52**, 1338.
49 R. R. Sharp, *J. Chem. Phys.*, 1972, **57**, 5321.
50 R. R. Sharp and J. W. Tolan, *J. Chem. Phys.*, 1976, **65**, 522.
51 D. M. Chan and T. B. Marder, *Angew. Chem., Int. Ed.*, 1988, **27**, 442.

 

52 N. Arnold, H. Braunschweig, P. Brenner, J. O. C. Jimenez-Halla, T. Kupfer and K. Radacki, *Organometallics*, 2012, **31**, 1897.
53 Z. Cerny, J. Machacek, J. Fusek, B. Casensky, O. Kriz and D. G. Tuck, *J. Chem. Soc., Dalton Trans.*, 1998, 1439.
54 R. M. Hawk and R. R. Sharp, *J. Chem. Phys.*, 1974, **60**, 1009.
55 R. M. Hawk and R. R. Sharp, *J. Chem. Phys.*, 1974, **60**, 1522.
56 M. Mantina, A. C. Chamberlin, R. Valero, C. J. Cramer and D. G. Truhlar, *J. Phys. Chem. A*, 2009, **113**, 5806.
57 B. Cordero, V. Gomez, A. E. Platero-Prats, M. Reves, J. Echeverria, E. Cremades, F. Barragan and S. Alvarez, *Dalton Trans.*, 2008, 2832.
58 H. Schmidbaur, T. Probst, B. Huber, O. Steigelmann and G. Müller, *Organometallics*, 1989, **8**, 1567.
59 H. Schmidbaur, T. Probst, B. Huber, G. Müller and C. Krueger, *J. Organomet. Chem.*, 1989, **365**, 53.
60 A. Jana, S. P. Sarish, H. W. Roesky, C. Schulzke, A. Doering and M. John, *Organometallics*, 2009, **28**, 2563.
61 D. Weber, S. H. Hausner, A. Eisengraeber-Pabst, S. Yun, J. A. Krause-Bauer and H. Zimmer, *Inorg. Chim. Acta*, 2004, **357**, 125.
62 S. Baba Haj, M. Schuermann, L. Iovkova-Berends, S. Herres-Pawlis and K. Jurkschat, *Organometallics*, 2012, **31**, 4716.
63 K. Eichkorn, O. Treutler, H. Ohm, M. Häser and R. Ahlrichs, *Chem. Phys. Lett.*, 1995, **242**, 652.
64 S. Grimme, J. Antony, S. Ehrlich and H. Krieg, *J. Chem. Phys.*, 2010, **132**, 154104.
65 S. Grimme, S. Ehrlich and L. Goerigk, *J. Comput. Chem.*, 2011, **32**, 1456.
66 (*a*) A. D. Becke, *Phys. Rev. A*, 1988, **38**, 3098; (*b*) J. P. Perdew, *Phys. Rev. B: Condens. Matter Mater. Phys.*, 1986, **33**, 8822.
67 F. Weigend and R. Ahlrichs, *Phys. Chem. Chem. Phys.*, 2005, **7**, 3297.
68 D. Heitmann, T. Pape, A. Hepp, C. Mück-Lichtenfeld, S. Grimme and F. E. Hahn, *J. Am. Chem. Soc.*, 2011, **133**, 11118.
69 A. E. Reed, L. A. Curtiss and F. Weinhold, *Chem. Rev.*, 1988, **88**, 899.
70 (*a*) M. P. Mitoraj, A. Michalak and T. Ziegler, *J. Chem. Theory Comput.*, 2009, **5**, 962; (*b*) T. Ziegler and A. Rauk, *Theor. Chim. Acta*, 1977, **46**, 1.
71 R. Tonner and G. Frenking, *Chem.–Eur. J.*, 2008, **14**, 3260.
72 P. Parameswaran and G. Frenking, *Chem.–Eur. J.*, 2009, **15**, 8807.
73 M. A. Celik, G. Frenking, B. Neumüller and W. Petz, *ChemPlusChem*, 2013, **78**, 1024.
74 C.-Y. Lin, J.-D. Guo, J. C. Fettinger, S. Nagase, F. Grandjean, G. J. Long, N. F. Chilton and P. P. Power, *Inorg. Chem.*, 2013, **52**, 13584.
75 TURBOMOLE V6.5 2013, a development of University of Karlsruhe and Forschungszentrum Karlsruhe GmbH, 1989–2007, TURBOMOLE GmbH, since 2007, Karlsruhe, 2013, http://www.turbomole.com.
76 G. Te Velde, F. M. Bickelhaupt, E. J. Baerends, C. Fonseca Guerra, S. J. A. van Gisbergen, J. G. Snijders and T. Ziegler, *J. Comput. Chem.*, 2001, **22**, 931.
77 J. G. Snijders, E. J. Baerends and P. Vernoojs, *At. Data Nucl. Data Tables*, 1982, **26**, 483.
78 E. van Lenthe, E. J. Baerends and J. G. Snijders, *J. Chem. Phys.*, 1993, **99**, 4597.